

Article

Natural Characteristics of a Marine Two-Stage Tandem Hybrid Planetary System

Xingfu Zhao ¹, Zongxiang Yue ² , Jianjun Qu ², Marmysh Dzianis ³ and Yanzhong Wang ^{1,*}

¹ School of Mechanical Engineering & Automation, Beihang University, Beijing 100083, China; xingfu_zhao2024@163.com

² School of Mechanics Engineering, Harbin Institute of Technology, Harbin 150001, China; yuezongxiang1121@163.com (Z.Y.); qujianjun@hit.edu.cn (J.Q.)

³ School of Mechanics and Mathematics, Belarusian State University, 220030 Minsk, Belarus; marmyshde@bsu.by

* Correspondence: yz_wang_bhu@163.com; Tel.: +86-166-2290-5373

Abstract: This study focuses on a marine two-stage tandem hybrid planetary system. Natural frequencies and vibration modes are determined using a translational–torsional coupled dynamic model. Based on the motion characteristics of the transmission system, free vibration is categorized into three typical modes. The parameter sensitivity of natural frequencies is computed, and the effects of structural parameters such as unequally spaced planet, mesh stiffness, planet mass and rotational inertia on the natural frequencies are analyzed. Utilizing the coupling factor, the mode transition criterion for the natural frequencies response to parameters is formulated. The results demonstrate that the vibration modes of the two-stage tandem hybrid planetary system can be classified as the fixed-axis train vibration mode, the differential train vibration mode, and the coupled vibration mode. Unequally spaced planet primarily disrupts vibration modes without significantly affecting natural frequencies. In contrast, the effects of mesh stiffness, planet mass and rotational inertia on the modes are opposite to those of unequally spaced planets. The validity of the parameter sensitivity and mode transition criterion is substantiated through illustrative examples.

Keywords: compound gear system; natural frequency; vibration mode; unequally spaced planet; mode transition



Citation: Zhao, X.; Yue, Z.; Qu, J.; Dzianis, M.; Wang, Y. Natural Characteristics of a Marine Two-Stage Tandem Hybrid Planetary System. *Machines* **2024**, *12*, 338. <https://doi.org/10.3390/machines12050338>

Academic Editor: Davide Astolfi

Received: 13 April 2024

Revised: 8 May 2024

Accepted: 10 May 2024

Published: 14 May 2024



Copyright: © 2024 by the authors. Licensee MDPI, Basel, Switzerland. This article is an open access article distributed under the terms and conditions of the Creative Commons Attribution (CC BY) license (<https://creativecommons.org/licenses/by/4.0/>).

1. Introduction

The development of marine trade puts more and more demands on the transmission of ships. The two-stage tandem hybrid planetary system studied in this paper is an important part of the ship's after-transmission. The whole system is a combination of herringbone-tooth fixed-axis train and differential train, which is the main source of vibration in ship machinery and equipment and has a great influence on the reliability of ship operation. Reducing the noise and vibration of the transmission system is of great significance in prolonging the service life of the ship and improving economic efficiency.

The study of natural characteristics is an important part of dynamic research, which has an important influence on the dynamic response of the system, the generation and transfer of dynamic loads, the form of system vibration, etc. In recent years, many scholars have carried out much meaningful research on the natural characteristics of gear systems. Ambarisha et al. [1,2] mainly studied the natural characteristics of helical planetary systems, which opened the prelude to the study of the natural characteristics of gear systems. Zhao et al. [3] carried out a sensitivity analysis based on the torsional dynamics of a wind turbine and found that the natural frequencies are very sensitive to the torsional stiffness of the shaft and the gear mesh stiffness. Zhang et al. [4] investigated the effects of the number of planet gears and coupling stiffness on the natural characteristics of closed planetary gear systems to analyze the dynamic response and avoid resonance. Wu et al. [5] investigated

the mode characteristics of equally spaced planets by using the perturbation method and the candidate modal method. Sondkar et al. [6] proposed a linear constant model for a double-helix planetary gear set by solving the corresponding eigenvalues. The natural characteristics were calculated by solving the corresponding eigenvalue problem. Hao et al. [7] developed a dynamic model of dual-power split gear transmission, solved the time-varying mesh stiffness of the model and obtained the natural characteristics by using the loaded tooth contact analysis (LTCA) technique. Cui et al. [8] developed a bending–torsion coupled dynamic model of a composite planetary gear transmission system for a vehicle, from which the system’s natural frequency and vibration mode characteristics of the system were extracted, and the effects of rotational inertia and mesh stiffness on the natural characteristics were investigated. Shuai et al. [9] developed a dynamic model of a herringbone planetary gear train based on the concentrated parameter theory and Lagrange’s method and investigated the effects of the flexible support and the floating of the sun gear on the natural frequencies. Mbarek et al. [10] analyzed the natural characteristics of a planetary gear train under different load conditions and mesh stiffness fluctuations and performed hammering tests to verify the correctness of the centralized parameter model. Cooley et al. [11] investigated the vibration modes and natural frequencies of high-speed planet gears with gyroscopic effects at very high speeds for the phenomena of dispersion and chattering instability. Qiu W et al. [12] established a dynamic model for a typical interlinked planetary gear system, considering translational vibration, torsional vibration and gyroscopic effects to investigate its free vibration characteristics. Liu H et al. [13] studied the modal characteristics of a two-stage planetary gear system (TSPG) with a short, intermediate shaft and applied modal energy analysis to quantify the importance of the intermediate shaft throughout the entire TSPG system. Hu Z et al. [14] proposed a dynamic model for a bifurcated torque split gear transmission system, obtaining the system’s natural characteristics, including natural frequencies and critical speeds. Huang C et al. [15] established a finite element modal analysis model for planetary reducers with small tooth number differences in ABAQUS, obtaining the natural frequencies and corresponding vibration modes of the reducer. Additionally, modal parameters were validated through modal hammer experiments conducted in the LMS Test.Lab. Hu C et al. [16] developed a translational–torsional dynamic model for a multistage planetary gear transmission system; subsequently, they investigated the influence of natural frequencies, mesh stiffness and component mass on the natural frequencies. Tatar A et al. [17] considered the gyroscopic effect and established a six-degree-of-freedom dynamic model of the planetary gear system with equally spaced planets, analyzing its modes.

Planet gears used in planetary gearboxes are usually equally spaced. However, unequal planet spacing can sometimes lead to positioning errors between the planet gears [18]. There are some studies related to this phenomenon. Tatar et al. [18] proposed a parametric study to determine the effect of design parameters, such as an unequally spaced planet, on the global modal behavior of a planetary gear rotor system. Guo et al. [19] investigated the sensitivity of the natural characteristics of a general planetary gear train to mass and stiffness parameters in response to tuning and unequal phenomena. Parker et al. [20] proved the highly structured modal characteristics of planet gears with unequally spaced planets and elastic ring gear and discussed the rules of how the modes of planet gears with equal spacing evolve with unequally spaced planets. Cooley et al. [21] defined an eigenvalue steering parameter and used it to analyze steering in high-speed planet gears, which is prominent in unequally spaced planetary gears.

Although there have been some studies on the natural characteristics of planetary gear systems, the two-stage tandem hybrid planetary system consisting of a fixed-axis train and a differential train has been studied to a lesser extent. In particular, the sensitivity of the natural frequencies to the gear parameters and the mode transition phenomena due to parameter variations in this system have not been explored in depth. For this purpose, this paper summarizes three typical vibration modes based on the centralized parametric model of a two-stage tandem hybrid planetary system and investigates the sensitivity of the

natural frequencies to unequally spaced planets, mesh stiffness, planet mass and rotational inertia, and the mode transition phenomenon under the influence of different parameters.

2. Dynamic Model of the Transmission System

A schematic diagram of the marine two-stage tandem hybrid planetary system is given in Figure 1. The entire system is composed of the central components (sun gears a and s , left ring gears dL , right ring gears dR , left ring gears rL , right ring gears rR , carriers c and h , and planet gears mi, pi), as well as the input shaft and output shaft. This transmission design incorporates a combination of fixed-axis and differential trains. The input power is divided into two segments within the system. A specific portion is designated for the fixed-axis train, flowing from the sun gear a to the ring gear d . Concurrently, the remaining section is allocated for the differential train, starting from the sun gear s and further distributed to the carrier h and ring gear r .

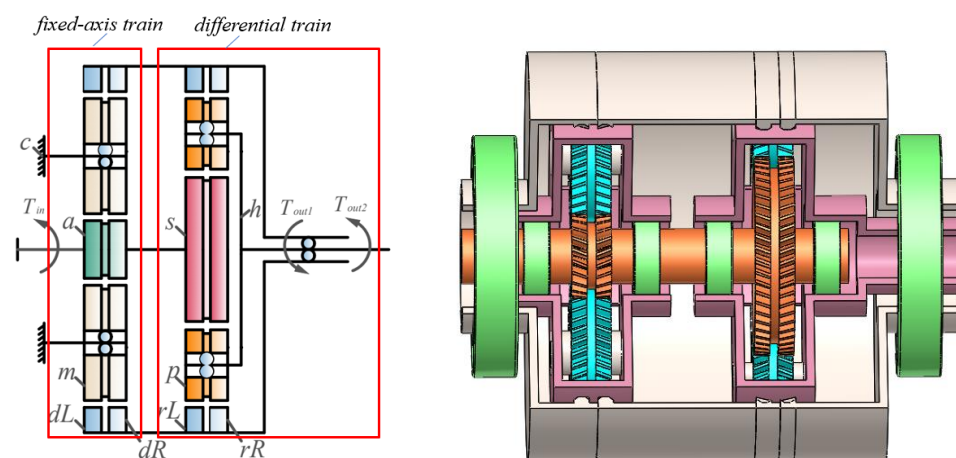


Figure 1. Schematic diagram of marine two-stage tandem hybrid planetary system.

The centralized parameter method is used, and the coupling between the fixed-axis train and the differential train is considered to establish the dynamic model of the two-stage tandem hybrid planetary system. The schematic diagram of the differential train model is shown in Figure 2, with detailed parameters shown in the reference [9].

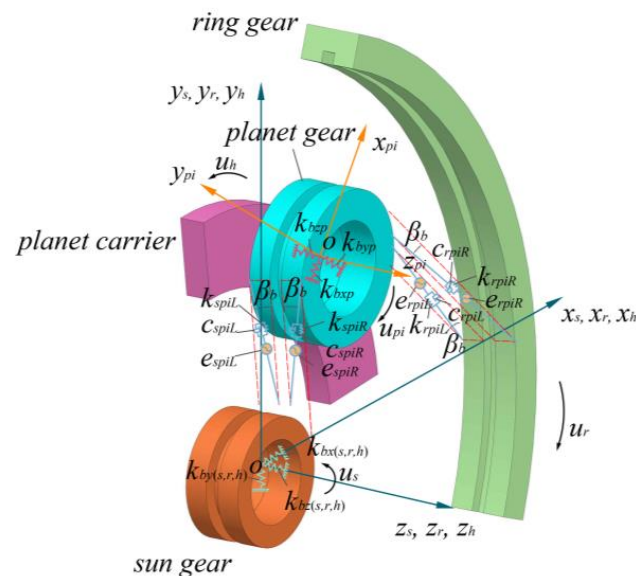


Figure 2. Dynamic model of the differential train.

In this model, the sun gear, planet gear, ring gear and planet carrier are assumed to be rigid, and the meshing of the gears is represented by linear springs acting on the tooth surfaces. The time-varying component of the mesh stiffness due to the variation in the meshing tooth pairs is neglected, and the average mesh stiffness is used to calculate the contact between the tooth surfaces.

Using the Lagrange's equations, the motion equations for a two-stage tandem hybrid planetary system can be written as:

$$\mathbf{M}\ddot{\mathbf{q}}(t) + \mathbf{C}\dot{\mathbf{q}}(t) + [\mathbf{K}_b + \mathbf{K}_m(t)]\mathbf{q}(t) = \mathbf{F}_t, \quad (1)$$

where \mathbf{q} is the generalized coordinate vector including transverse, axial and torsional motions; \mathbf{M} is the mass matrix; \mathbf{C} is the damping matrix; \mathbf{K}_b is the bearing support stiffness matrix; \mathbf{K}_m is the mesh stiffness matrix; and \mathbf{F}_t is the vector of internal and external excitation forces due to the combined drive and load moments and mesh errors.

$$\ddot{\mathbf{q}} = [x_j, y_j, z_j, \theta_{zj}] \quad (j = a, dL, dR, m1, \dots, m3, s, h, rL, rR, p1, \dots, p3) \quad (2)$$

$$\mathbf{M} = \text{diag}[M_j, M_j, M_j, J_j] \quad (j = a, dL, dR, m1, \dots, m3, s, h, rL, rR, p1, \dots, p3) \quad (3)$$

where x_j , y_j , z_j , and θ_{zj} represent the displacements of component j in the transverse direction, axial direction and torsional direction, respectively. M_j is the mass matrix of component j .

$$\mathbf{C} = [\mathbf{C}_a \ \mathbf{C}_{dL} \ \mathbf{C}_{dR} \ \mathbf{C}_m \ \mathbf{C}_s \ \mathbf{C}_h \ \mathbf{C}_{rL} \ \mathbf{C}_{rR} \ \mathbf{C}_p], \quad (4)$$

$$\mathbf{K} = \mathbf{K}_b + \mathbf{K}_m = [\mathbf{K}_a \ \mathbf{K}_{dL} \ \mathbf{K}_{dR} \ \mathbf{K}_m \ \mathbf{K}_s \ \mathbf{K}_h \ \mathbf{K}_{rL} \ \mathbf{K}_{rR} \ \mathbf{K}_p], \quad (5)$$

3. Mode Analysis

According to the dynamic model of the system, the undamped free vibration equation is obtained as follows:

$$\mathbf{M}\ddot{\mathbf{q}}(t) + [\mathbf{K}_b + \mathbf{K}_m(t)]\mathbf{q}(t) = 0, \quad (6)$$

The dynamic equation corresponds to the characteristic equation:

$$[(\mathbf{K}_b + \mathbf{K}_m) - w_i^2 \mathbf{M}]\phi_i = 0, \quad (7)$$

where w_i is the i -th order natural frequency and ϕ_i is the i -th order mode.

To quantify the mode sensitivity, the frequency shift between the two extreme cases is calculated as follows [17]:

$$\text{frequency shift}(\%) = \frac{|w_i - w_f|}{w_i} \times 100, \quad (8)$$

where w_i and w_f represent the initial and final natural frequencies.

All planets have the same model parameters in the fixed-axis train and the differential train. Table 1 lists the main system parameters. Using numerical methods, the natural frequencies and vibration modes can be calculated (the tables are in Appendices). The vibration modes of the system can be categorized into three types: (1) fixed-axis train vibration mode; (2) differential train vibration mode; (3) coupled vibration mode.

Table 1. Parameters of the marine two-stage tandem hybrid planetary system.

Item	Number of Teeth	Angle of Helix (°)	Normal Pressure Angle (°)	Module	Mass (kg)	Rotational Inertia (kg·mm ²)
Sun gear <i>a</i>	22	20	20	1.5	0.092	17.664
Planet gear <i>m</i>	44	20	20	1.5	0.327	268.521
Ring gear <i>dL</i>	110	20	20	1.5	0.163	1325.860
Ring gear <i>dR</i>	110	20	20	1.5	0.163	1325.860
Sun gear <i>s</i>	55	20	20	1.5	0.488	525.752
Planet gear <i>p</i>	27	20	20	1.5	0.108	35.531
Ring gear <i>rL</i>	110	20	20	1.5	0.163	1325.860
Ring gear <i>rR</i>	110	20	20	1.5	0.163	1325.860
Planet carrier <i>h</i>	/	/	/	/	1.648	4946.014

3.1. Fixed-Axis Train Vibration Mode

The fixed-axis vibration mode satisfies the following characteristics:

- (1) The vibration displacements of the sun gear, ring gear, planet gears and planet carrier in the differential train are zero.
- (2) The corresponding multiple roots of the natural frequency are 2, with a total of 7 pairs.
- (3) The fixed-axis train has no axial and torsional motion, and the vibration modes of the central component corresponding to the frequencies ϕ_i and $\bar{\phi}_i$ are:

$$\mathbf{p}_j = [x_j, y_j, 0, 0], \bar{\mathbf{p}}_j = [-y_j, x_j, 0, 0], j = (a, dL, dR), \tag{9}$$

The corresponding planet gear vibration modes have the following relationships:

$$\begin{bmatrix} \mathbf{p}_{mn} \\ \bar{\mathbf{p}}_{mn} \end{bmatrix} = \begin{bmatrix} \cos \psi_n \mathbf{I} & -\sin \psi_n \mathbf{I} \\ \sin \psi_n \mathbf{I} & \cos \psi_n \mathbf{I} \end{bmatrix} \begin{bmatrix} \mathbf{p}_{m1} \\ \bar{\mathbf{p}}_{m1} \end{bmatrix}, \tag{10}$$

The vibration modes can be expressed in the following form:

$$\begin{aligned} \phi_i &= [\mathbf{p}_a, \mathbf{p}_{dL}, \mathbf{p}_{dR}, \cos \psi_1 \mathbf{p}_{m1} - \sin \psi_1 \bar{\mathbf{p}}_{m1}, \dots, \cos \psi_n \mathbf{p}_{m1} - \sin \psi_n \bar{\mathbf{p}}_{m1}]^T \\ \bar{\phi}_i &= [\bar{\mathbf{p}}_a, \bar{\mathbf{p}}_{dL}, \bar{\mathbf{p}}_{dR}, \sin \psi_1 \mathbf{p}_{m1} + \cos \psi_1 \bar{\mathbf{p}}_{m1}, \dots, \sin \psi_n \mathbf{p}_{m1} + \cos \psi_n \bar{\mathbf{p}}_{m1}]^T, \end{aligned} \tag{11}$$

A schematic diagram of the fixed-axis train vibration mode is given in Figure 3.

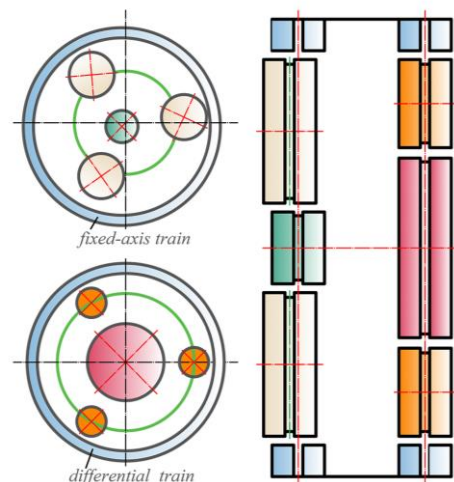


Figure 3. Fixed-axis train vibration mode.

3.2. Differential Train Vibration Mode

Similar to the fixed-axis train, the differential train vibration mode satisfies the following characteristics:

- (1) The vibration displacements of the sun gear, ring gear and planet gears in the fixed-axis train are zero.
- (2) The corresponding multiple roots of the natural frequency are 2, with a total of 8 pairs.
- (3) The differential train has no axial and torsional motion, and the vibration modes of the central components corresponding to the frequencies ϕ_i and $\bar{\phi}_i$ are:

$$\mathbf{p}_j = [x_j, y_j, 0, 0], \bar{\mathbf{p}}_j = [-y_j, x_j, 0, 0], j = (s, rL, rR, h), \tag{12}$$

The corresponding planet gear vibration modes have the following relationships:

$$\begin{bmatrix} \mathbf{p}_{pn} \\ \bar{\mathbf{p}}_{pn} \end{bmatrix} = \begin{bmatrix} \cos \psi_n \mathbf{I} & -\sin \psi_n \mathbf{I} \\ \sin \psi_n \mathbf{I} & \cos \psi_n \mathbf{I} \end{bmatrix} \begin{bmatrix} \mathbf{p}_{p1} \\ \bar{\mathbf{p}}_{p1} \end{bmatrix}, \tag{13}$$

where \mathbf{I} is the 3rd-order unit matrix.

The vibration modes can be expressed in the following form:

$$\begin{aligned} \phi_i &= [\mathbf{p}_s, \mathbf{p}_{rL}, \mathbf{p}_{rR}, \mathbf{p}_h, \cos \psi_1 \mathbf{p}_{p1} - \sin \psi_1 \bar{\mathbf{p}}_{p1}, \dots, \cos \psi_n \mathbf{p}_{p1} - \sin \psi_n \bar{\mathbf{p}}_{p1}]^T \\ \bar{\phi}_i &= [\bar{\mathbf{p}}_s, \bar{\mathbf{p}}_{rL}, \bar{\mathbf{p}}_{rR}, \bar{\mathbf{p}}_h, \sin \psi_1 \mathbf{p}_{p1} + \cos \psi_1 \bar{\mathbf{p}}_{p1}, \dots, \sin \psi_n \mathbf{p}_{p1} + \cos \psi_n \bar{\mathbf{p}}_{p1}]^T, \end{aligned} \tag{14}$$

A schematic diagram of the differential train vibration mode is given in Figure 4.

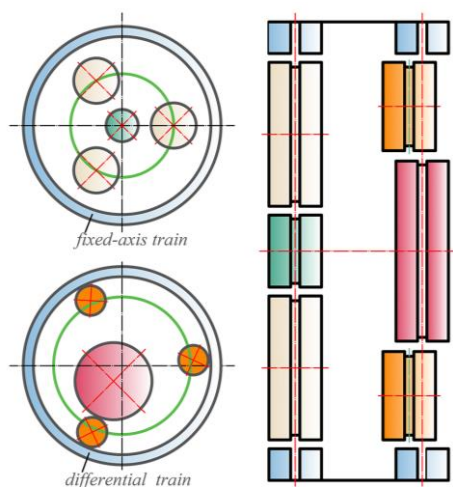


Figure 4. Differential train vibration mode.

3.3. Coupled Vibration Mode

The coupled vibration mode satisfies the following characteristics:

- (1) The corresponding natural frequencies are single roots, with a total of 22.
- (2) There are no transverse motions of the central components in the fixed-axis train and the differential train, and the vibration modes of the respective planet gears in the two systems are the same.
- (3) The coupled vibration modes include a planet carrier axial vibration mode and ring gears torsional vibration mode, corresponding to the number of natural frequencies of 1 and 2, respectively, which also satisfy the characteristics of the coupled vibration modes and can be regarded as a special coupled vibration mode.

The vibration modes of the central components are as follows:

$$\mathbf{p}_j = [0, 0, z_j, \theta_{zj}] j = (a, dL, dR, s, rL, rR, h), \tag{15}$$

The planet gear vibration modes have the following relationship:

$$\mathbf{p}_{mn} = \mathbf{p}_{m1} = [x_{m1}, y_{m1}, z_{m1}, \theta_{zm1}], \mathbf{p}_{pn} = \mathbf{p}_{p1} = [x_{p1}, y_{p1}, z_{p1}, \theta_{zp1}], \quad (16)$$

The vibration modes can be expressed in the following form:

$$\phi_i = [\mathbf{p}_a, \mathbf{p}_{dL}, \mathbf{p}_{dR}, \mathbf{p}_{m1}, \dots, \mathbf{p}_{mn}, \mathbf{p}_s, \mathbf{p}_{rL}, \mathbf{p}_{rR}, \mathbf{p}_h, \mathbf{p}_{p1}, \dots, \mathbf{p}_{pn}]^T, \quad (17)$$

A schematic diagram of the coupled vibration mode is given in Figure 5.

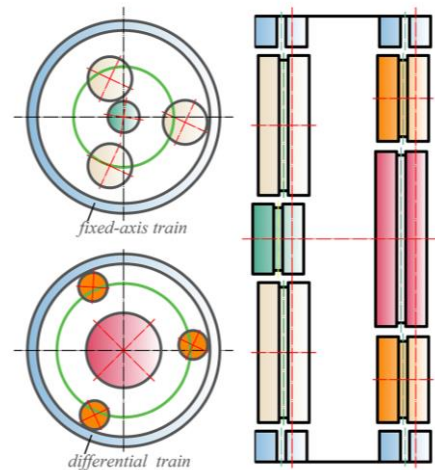


Figure 5. Coupled vibration mode.

3.4. Verification of the Mathematical Model Using the Finite Element Method

Reference [22] utilized the finite element method to calculate the natural frequencies of the 2K-H planetary gear system and compared the results with a mathematical model. To validate the mathematical model of the paper, a finite element model was employed. Based on the parameters in Table 1, the transmission system was accurately modeled using the three-dimensional modeling software Solidworks(2018). Subsequently, ANSYS Workbench(2020) was utilized for mesh generation, dividing the transmission system into a total of 131,027 nodes and 56,674 elements. Appropriate boundary and loading conditions were set, as shown in Figure 6. The first six vibration modes were extracted, and the obtained vibration modes and frequencies are presented in Table 2.

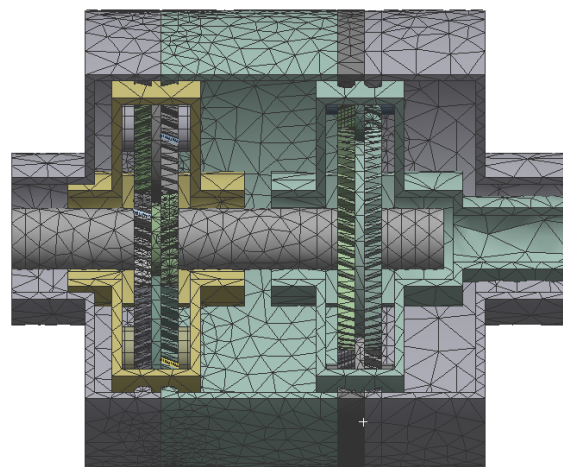


Figure 6. The finite element model of the marine two-stage tandem hybrid planetary system.

Table 2. Comparison of vibration modes obtained from two models.

Mode	Mathematical Model Nat. Freq. (Hz)	Finite Element Model Nat. Freq. (Hz)	Difference (%)	Mod Type
1	0	0	0	/
2	249.96	255.71	2.3	couple
3	538.75	564.61	4.8	couple
4	680.52	656.02	−3.6	differential train
5	680.52	656.02	−3.6	differential train
6	1005.47	1031.6	2.6	fixed-axis train

Table 2 reveals that, among the first six natural frequencies, the maximum difference between the finite element model and the mathematical model is 4.8%. The obtained vibration types are also consistent. Therefore, the finite element analysis results are in good agreement with the mathematical model, validating the effectiveness of the mathematical model.

4. Sensitivity Analysis of Natural Frequency

The study of the sensitivity of the natural frequencies to the system parameters can provide an important basis for the reduction in the system response and the optimization of the structural design. The sensitivity analysis of natural frequencies focuses on the effect of gear parameters on natural frequencies and vibration modes. The parameters include unequally spaced planet, mesh stiffness, planet mass and rotational inertia.

The characteristic sensitivity of the free vibration of the system shown in Equation (7) can be obtained by the following expressions:

(1) When the eigenvalue is a single root, the eigenvalue sensitivity is given by

$$\lambda'_i = \phi_i^T (K' - \lambda_i M') \phi_i, \quad (18)$$

(2) When the eigenvalue is a repeated root, the eigenvalue sensitivity can be obtained by solving for the eigenvalue of the following equation:

$$D a_i = \lambda'_i a_i, D = \Gamma^T (K' - \lambda_i M') \Gamma, \quad (19)$$

where Γ represents a set of m -dimensional vectors, m is the number of repeated roots, and the following relationship holds:

$$\Gamma^T M \Gamma = I_{m \times m}, \quad (20)$$

$$\phi_i = \Gamma a_i \quad (21)$$

4.1. Unequally Spaced Planets

For the convenience of the study, the deviation angle of the first planet gear from its original position in the fixed-axis train and differential train was set to range from 0° to 15° , respectively. The frequency shifts of the first 25 modes were calculated, as shown in Table 3. The sensitivity of the first 25 natural frequencies to the inequality is shown in Figure 7. The frequency shifts for deviation angle = 0° and deviation angle = 15° are shown in Figure 8.

Table 3. Vibration modes for planet gears are unequally spaced.

Mode	Dev. Ang. = 0°		Fixed-Axis Train			Differential Train		
	Nat. Freq. (Hz)	Mod Type	Dev. Ang. = 15° Nat. Freq. (Hz)	Dev. Ang. = 15° Mod Type	Freq. Shift(%)	Dev. Ang. = 15° Nat. Freq. (Hz)	Dev. Ang. = 15° Mod Type	Freq. Shift (%)
1	0	couple	0	global	0	0	couple-global	0
2	249.96	couple	249.96	global	0	248.81	couple-global	0.46
3	538.75	couple	538.12	global	0.12	538.74	couple-global	0
4	680.52	differential train	673.84	global	0.98	634.64	couple-global	6.74
5	680.52	differential train	688.91	global	1.23	718.85	couple-global	5.63
6	1005.47	fixed-axis train	1000.53	global	0.49	1005.47	fixed-axis train	0
7	1005.47	fixed-axis train	1005.87	global	0.04	1005.47	fixed-axis train	0
8	1138.42	planet carrier	1138.42	planet carrier	0	1138.42	planet carrier	0
9	1385.93	couple	1385.6	global	0.02	1385.85	couple-global	0.01
10	1497.41	couple	1495.52	global	0.13	1497.12	couple-global	0.02
11	2030.67	couple	2029.86	global	0.04	2030.03	couple-global	0.03
12	2054.77	couple	2044	global	0.52	2053.98	couple-global	0.04
13	2292.34	differential train	2266.85	global	1.11	2285.13	couple-global	0.31
14	2292.34	differential train	2306.73	global	0.63	2294.74	couple-global	0.1
15	2504.67	differential train	2458.41	global	1.85	2477.16	couple-global	1.1
16	2504.67	differential train	2552.05	global	1.89	2528.65	couple-global	0.96
17	2809.75	fixed-axis train	2749.92	global	2.13	2809.75	fixed-axis train	0
18	2809.75	fixed-axis train	2837.37	global	0.98	2809.75	fixed-axis train	0
19	2938.39	couple	2938.39	global	0	2934.2	couple-global	0.14
20	3169.47	differential train	3169.39	global	0	3113.13	couple-global	1.78
21	3169.47	differential train	3169.55	global	0	3225.96	couple-global	1.78
22	4288.77	differential train	4243.9	global	1.05	4134.17	couple-global	3.6
23	4288.77	differential train	4331.34	global	0.99	4420.11	couple-global	3.06
24	4507.93	couple	4508.32	global	0.01	4508.21	couple-global	0.01
25	5388.32	couple	5307.26	global	1.5	5388.33	couple-global	0

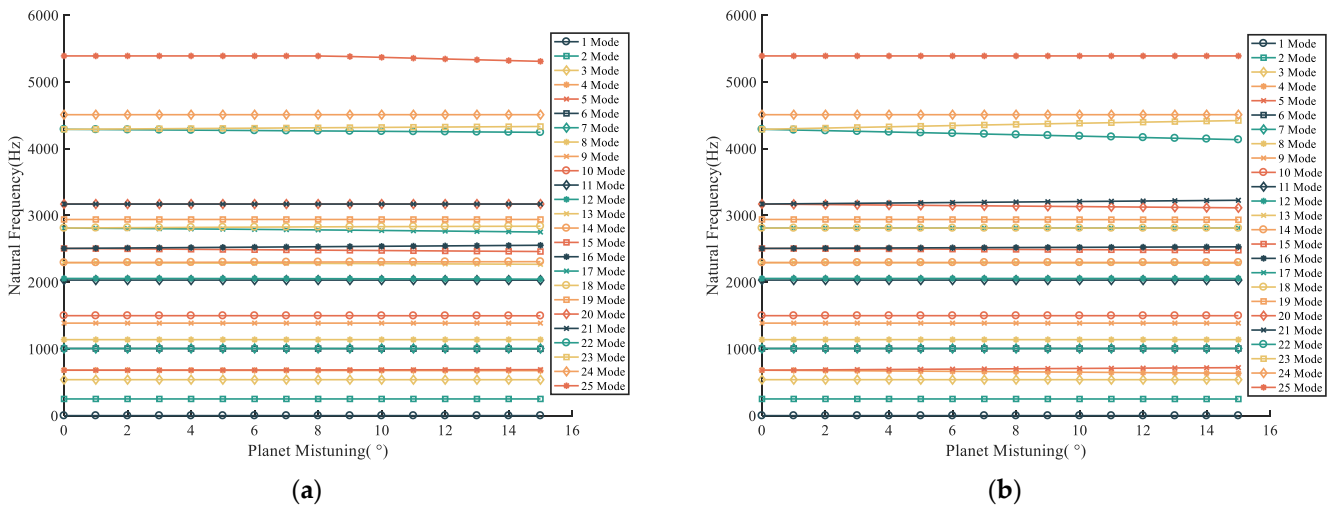


Figure 7. Sensitivity of the first 25 natural frequencies to the unequally spaced planet: (a) unequally spaced planet of a fixed-axis train; (b) unequally spaced planet of a differential train.

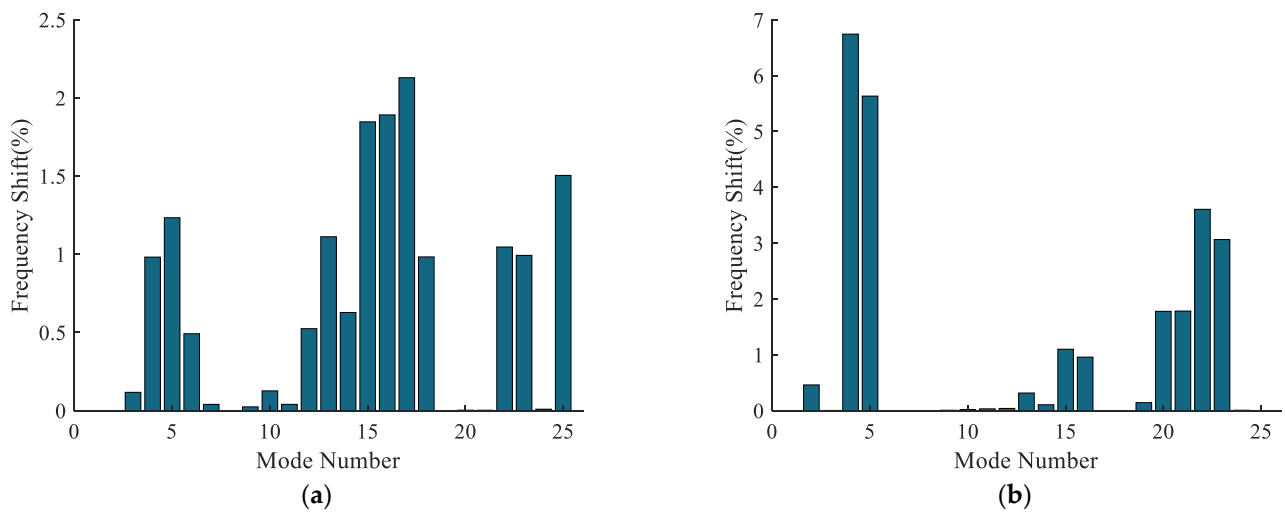


Figure 8. Frequency shifts for deviation angle = 0° and deviation angle = 15° : (a) unequally spaced planet of a fixed-axis train; (b) unequally spaced planet of a differential train.

From Table 3 and Figures 6 and 7, it can be seen that when the planet gears of the fixed-axis train and the differential train are unequally spaced, the first 25 natural frequencies are not very sensitive to the deviation angles. The maximum frequency shift is not more than 7% in both unequally spaced planets. However, it can be observed from Table 3 that the change in vibration modes is large. When the planet gear of the fixed-axis train is unequally spaced, except for the 8th-order planet carrier axial vibration mode, which remains unchanged, the vibration modes are transformed into global vibration modes. (In this vibration mode, vibration may exist in all directions with no obvious pattern.) When the planet gear of the differential train is unequally spaced, except for the 8th-order planet carrier axial vibration mode, the 6th-, 7th- and 17th- and 18th-order fixed-axis train vibration modes remain unchanged, and the rest of the vibration modes are transformed into the coupled-global vibration modes. (In this vibration mode, the fixed-axis train maintains the characteristics of the original coupling vibration mode, and the vibration of the gears of the differential train may be found in all directions without any obvious pattern.)

Since the unequally spaced planets break the cyclic symmetry of the two-stage tandem hybrid planetary system, the vibration modes are no longer easy to summarize, and new global vibration modes and coupled-global vibration modes appear. The unequally spaced planet in a fixed-axis gear train is more serious in damaging the vibration modes than that in a differential gear train. Because the latter still retains part of the original vibration pattern, the former is in addition to the planet carrier axial vibration mode; the vibration modes of the rest orders are changed to irregular global vibration modes.

In conclusion, the change in the natural frequencies caused by unequally spaced planets is very small, but the breakup of the vibration modes is more serious, and new global vibration modes and coupled-global vibration modes appear.

4.2. Mesh Stiffness

This section focuses on the influence of the mesh stiffness of sun gear–planet gear on the modes in the two-stage tandem hybrid planetary system. It is mainly divided into mesh stiffness sensitivity analysis and mode transition.

4.2.1. Mesh Stiffness Sensitivity Analysis

Taking the meshing stiffness of the sun gear–planet gear in the fixed-axis train k_{am} as an example, the sensitivity of the natural frequencies to the meshing stiffness was studied. It is categorized into the following cases:

- (1) Fixed-axis train vibration mode.

In the fixed-axis gear train vibration mode, the eigenvalues are multiple roots. Let the two eigenvalues be λ_1, λ_2 and $\lambda = \omega^2$, which are the eigenvalues of the matrix \mathbf{D} . \mathbf{D} is given by the following formula:

$$\mathbf{D} = \Gamma^T \mathbf{K}' \Gamma = \sum_{n=1}^N \begin{bmatrix} [(\delta_{amn})_1]^2 & (\delta_{amn})_1 (\delta_{amn})_2 \\ (\delta_{amn})_1 (\delta_{amn})_2 & [(\delta_{amn})_2]^2 \end{bmatrix}, \tag{22}$$

where δ_{amn} is the relative displacement between the n -th planet gear m and the sun gear a .

(2) Differential train vibration mode.

In the differential train vibration mode, $\delta_{amn} = 0$, so the sensitivity of the natural frequencies is zero.

(3) Coupled vibration mode.

In the coupled vibration mode, the eigenvalues are single roots, and the deformations of each planet gear are the same:

$$\lambda'_i = N[(\delta_{am1})_i]^2, \tag{23}$$

Similarly, the sensitivity of the natural frequencies to the mesh stiffness of sun gear-planet gear in the differential train k_{sp} can be obtained, which is similar to the above derivation and is not repeated here.

Briefly, with the change in k_{am} , the natural frequencies of the fixed-axis train vibration mode and the coupled vibration mode change, while the frequencies of the differential train vibration mode remain unchanged. With the change in k_{sp} , the frequencies of the differential train vibration mode and coupled vibration mode change, while the frequencies of the fixed-axis train vibration mode remain unchanged.

4.2.2. Mode Transition Criterion

When the system parameters are changed, the natural frequency curves approach gradually and then separate rapidly with a large curvature at a very close distance, a phenomenon known as mode transition [14]. Take k_{am} as an example to study the mode transition of natural frequency to mesh stiffness. It is categorized into the following cases:

(1) The corresponding modes of λ_r and λ_s are both fixed-axis train vibration modes.

In this case, both λ_r and λ_s are double roots, $\lambda_r = \lambda_p$ and $\lambda_s = \lambda_q$, and the coupling factors are calculated as follows:

$$\chi_r = \chi_p = -\chi_s = -\chi_q = \frac{2N^2}{\lambda_r - \lambda_s} [((\delta_{am1})_r (\delta_{am1})_s)^2 + ((\delta_{am1})_r (\delta_{am1})_q)^2 + ((\delta_{am1})_p (\delta_{am1})_s)^2 + ((\delta_{am1})_p (\delta_{am1})_q)^2], \tag{24}$$

When the coupling factor is 0, the natural frequencies undergo a mode transition; otherwise, they intersect. Bringing in the characteristics of the fixed-axis train vibration mode, it can be seen that the coupling factor can not be 0. Therefore, the natural frequencies, in this case, transition.

(2) The corresponding modes of λ_r and λ_s are both differential train modes.

In the differential train vibration mode, the fixed-axis train does not vibrate, the natural frequencies have zero sensitivity to k_{am} , and the trajectories of natural frequencies are straight lines. Therefore, the natural frequencies will not transition and intersect when k_{am} changes.

(3) The corresponding modes of λ_r and λ_s are coupled vibration modes.

In this case, both λ_r and λ_s are single roots, and the coupling factors are calculated as follows:

$$\chi_r = \frac{2(N(\delta_{am1})_r (\delta_{am1})_s)^2}{\lambda_r - \lambda_s} = -\chi_s, \tag{25}$$

Bringing in the characteristics of the coupled vibration mode, it can be seen that the coupling factors cannot be 0. Therefore, the natural frequencies, in this case, transition.

(4) λ_r belongs to the differential train vibration mode.

In this case, there is $\delta_{amn} = 0$. Therefore, the natural frequencies under the differential train vibration mode intersect with those under other vibration modes.

(5) λ_r belongs to the coupled vibration mode, and λ_s belongs to the fixed-axis train vibration mode.

In this case, λ_s are double roots, $\lambda_s = \lambda_q$, and the coupling factors are calculated as follows:

$$\begin{cases} \chi_s = \frac{2}{\lambda_s - \lambda_r} \left(\sum_{n=1}^N (\delta_{amn})_s (\delta_{amn})_r \right) 2 \\ \chi_q = \frac{2}{\lambda_s - \lambda_r} \left(\sum_{n=1}^N (\delta_{amn})_q (\delta_{amn})_r \right) 2 \\ \chi_r = -(\chi_s + \chi_q) \end{cases} \quad (26)$$

Bringing in the characteristics of the two vibration modes shows that $\chi_r = \chi_s = \chi_q = 0$ holds true, and therefore, the natural frequencies intersect.

Similarly, the mode transition criterion of the natural frequencies to k_{sp} can be obtained. The obtained mode transition criterion is summarized as shown in Table 4.

Table 4. Mode transition criterion of natural frequency to mesh stiffness.

	Vibration Mode	Meshing Stiffness k_{am} Mode Transition Criterion	Meshing Stiffness k_{sp} Mode Transition Criterion
Case1	All vibration modes are fixed-axis train vibration modes	transition	unchange
Case2	All vibration modes are differential train vibration modes	unchange	transition
Case3	All vibration modes are coupled vibration modes	transition	transition
Case4	Vibration modes are coupled vibration mode and fixed-axis train vibration mode	intersect	intersect
Case5	Vibration modes are coupled vibration mode and differential train vibration mode	intersect	intersect
Case6	Vibration modes are fixed-axis train vibration mode and differential train vibration mode	intersect	intersect

4.2.3. Sensitivity and Modal Transition Verification

The k_{am} and k_{sp} were set to be from 10^7 N/m to 10^8 N/m, respectively. The frequency shifts of the first 25 modes were calculated, as shown in Table 5. The sensitivity of the first 25 natural frequencies to the mesh stiffness is shown in Figure 9, and the frequency shifts for mesh stiffness of 10^7 N/m and 10^8 N/m are shown in Figure 10.

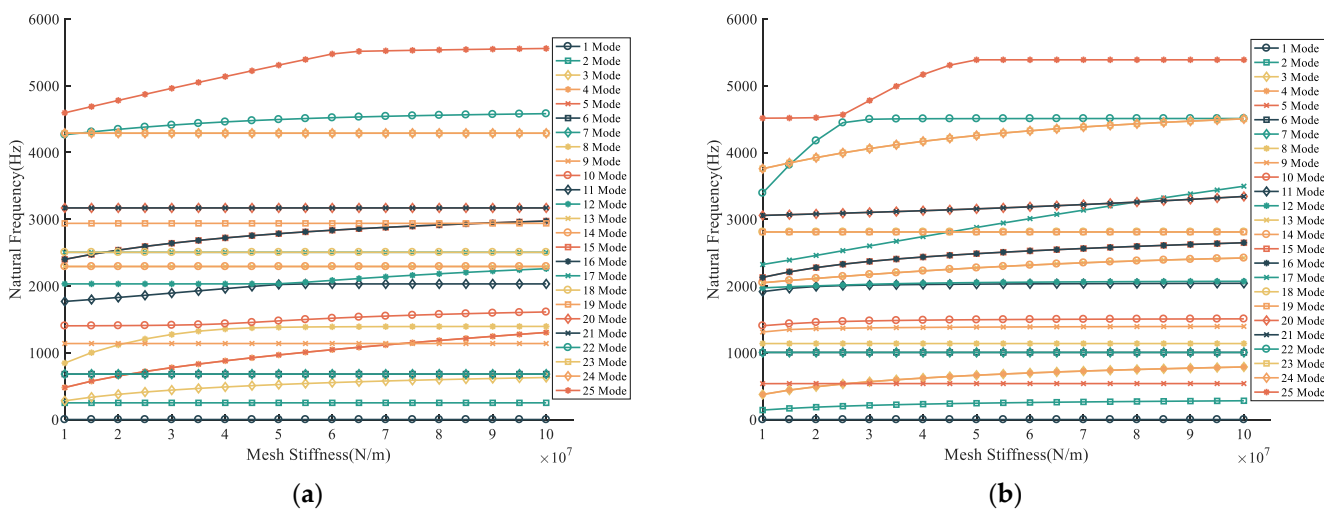


Figure 9. Sensitivity of the first 25 natural frequencies to the mesh stiffness: (a) k_{am} ; (b) k_{sp} .

Table 5. Vibration modes under variation in mesh stiffness.

Mode	Fixed-Axis Train				Differential Train			
	$k_{am} = 10^7$ N/m Nat. Freq. (Hz)	$k_{am} = 10^8$ N/m Nat. Freq. (Hz)	Mod Type	Freq. Shift (%)	$k_{sp} = 10^7$ N/m Nat. Freq. (Hz)	$k_{sp} = 10^8$ N/m Nat. Freq. (Hz)	Mod Type	Freq. Shift (%)
1	0	0	couple	0	0	0	couple	0
2	249.74	249.97	couple	0.09	142.13	281.43	couple	98.01
3	280.62	629.29	couple	124.25	375.67	787.68	differential train	109.67
4	479.39	1304.38	fixed-axis train	172.09	375.67	787.68	differential train	109.67
5	479.39	1304.38	fixed-axis train	172.09	537.79	538.86	couple	0.2
6	680.52	680.52	differential train	0	1005.47	1005.47	differential train	0
7	680.52	680.52	differential train	0	1005.47	1005.47	differential train	0
8	845.65	1394.85	couple	64.94	1138.42	1138.42	planet carrier	0
9	1138.42	1138.42	planet carrier	0	1311.12	1395.07	couple	6.4
10	1403.53	1611.29	couple	14.8	1405.05	1508.04	couple	7.33
11	1768.45	2031.44	couple	14.87	1916.28	2040.61	couple	6.49
12	2031.58	2259.49	couple	11.22	1972.24	2071.08	couple	5.01
13	2292.34	2292.34	differential train	0	2049.22	2420.15	differential train	18.1
14	2292.34	2292.34	differential train	0	2049.22	2420.15	differential train	18.1
15	2399.26	2973.19	fixed-axis train	23.92	2129.58	2648.16	differential train	24.35
16	2399.26	2973.19	fixed-axis train	23.92	2129.58	2648.16	differential train	24.35
17	2504.67	2504.67	differential train	0	2322.19	3495.13	couple	50.51
18	2504.67	2504.67	differential train	0	2809.75	2809.75	differential train	0
19	2938.38	2938.39	couple	0	2809.75	2809.75	differential train	0
20	3169.47	3169.47	differential train	0	3057.45	3341.41	differential train	9.29
21	3169.47	3169.47	differential train	0	3057.45	3341.41	differential train	9.29
22	4265.82	4581.29	couple	7.4	3392.91	4509.21	couple	32.9
23	4288.77	4288.77	differential train	0	3756.92	4503.96	differential train	19.88
24	4288.77	4288.77	differential train	0	3756.92	4503.96	differential train	19.88
25	4593.9	5557.98	couple	20.99	4514.16	5388.37	couple	19.37

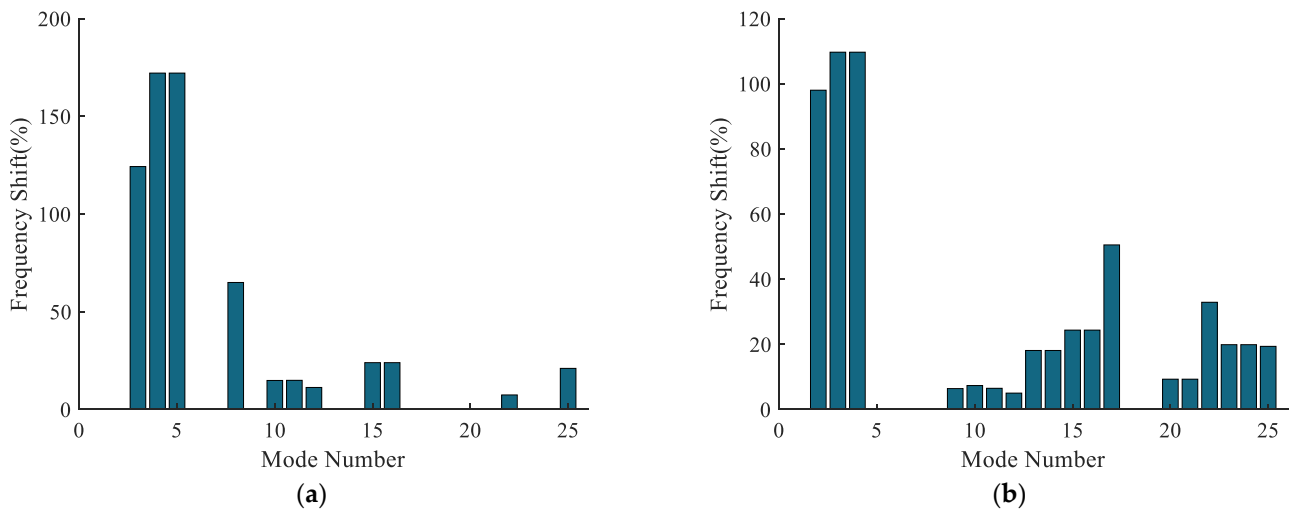


Figure 10. Frequency shifts for mesh stiffness of 10^7 N/m and 10^8 N/m: (a) k_{am} ; (b) k_{sp} .

From Table 5 and Figures 8 and 9, it can be seen that the influence of the mesh stiffness of the sun gear–planet gear on the natural frequencies is very large, and the frequency shift even reaches 172.09%. When k_{am} changes, the vibration modes corresponding to the changed natural frequencies are fixed-axis train vibration mode and coupled vibration mode; when k_{sp} changes, the vibration modes corresponding to the changed natural frequencies are differential train vibration mode and coupled vibration mode. This also verifies the sensitivity of the natural frequencies to the mesh stiffness in Section 4.2.1. Since there are more differential train vibration modes than fixed-axis train vibration modes in the first 25 modes, although the peak frequency shift generated by k_{am} is greater than that by k_{sp} , its influence affects fewer orders than k_{sp} .

The mode transition phenomenon can be observed in Figure 9, and the mode transition in Figure 9a is verified by comparing the mode transition criterion in Table 4. There is no case1 in Figure 9a; frequencies (13, 14) are a double root, belonging to the differential train vibration mode, which are straight lines, verifying case2; frequencies (11, 12) are two single roots, belonging to the coupled vibration mode, and the transitions occur at 5×10^7 N/m, verifying case3; frequencies (15, 16) are a double root, belonging to the fixed-axis train vibration mode; frequency (19) is a single root, belonging to the coupled vibration mode, and intersections occur at 9×10^7 N/m, verifying case4; there is no case5 in Figure 9a; frequencies (4, 5) are a double root, belonging to the fixed-axis train vibration mode, frequencies (6, 7) are a double root, belonging to the differential train vibration mode, and intersections occur at 2.5×10^7 N/m, verifying case6. The mode transitions and intersections occurring at other positions in Figure 9a also conform to the mode transition criterion in Table 4, and similarly, the mode transitions and intersections in Figure 9b can be verified to conform to the mode transition criterion, which is not repeated here.

In conclusion, the mesh stiffness of the sun gear–planet gear mainly affects the natural frequencies of the system and does not change the original vibration modes. The mode transitions and intersections that occur are also consistent with the formulated mode transition criterion.

4.3. Planet Mass

The study of the sensitivity of the natural frequencies to the planet mass/rotational inertia is similar to the methodology of Sections 4.2.1 and 4.2.2, which is not repeated here due to space implications. The mode transition criterion for the natural frequencies to the planet gear mass/rotational inertia is consistent with Table 4. The variation rule of the sensitivity of natural frequencies to planet mass/rotational inertia was obtained as follows:

As the planet gear mass M_m /rotational inertia J_m in the fixed-axis train changes, the natural frequencies of the fixed-axis train vibration mode and the coupled vibration mode change, while the natural frequencies of the differential train vibration mode remain unchanged. As the planet gear mass M_p /rotational inertia J_p in the differential train changes, the natural frequencies of the differential train vibration mode and the coupled vibration mode change, while the natural frequencies of the fixed-axis train vibration mode remain unchanged.

Setting M_m and M_p from 0.1 kg to 1 kg, respectively, the frequency shifts of the first 25 modes were calculated, as shown in Table 6. The sensitivity of the first 25 natural frequencies to the planet mass is shown in Figure 11, and the frequency shifts for planet mass of 0.1 kg and 1 kg are shown in Figure 12.

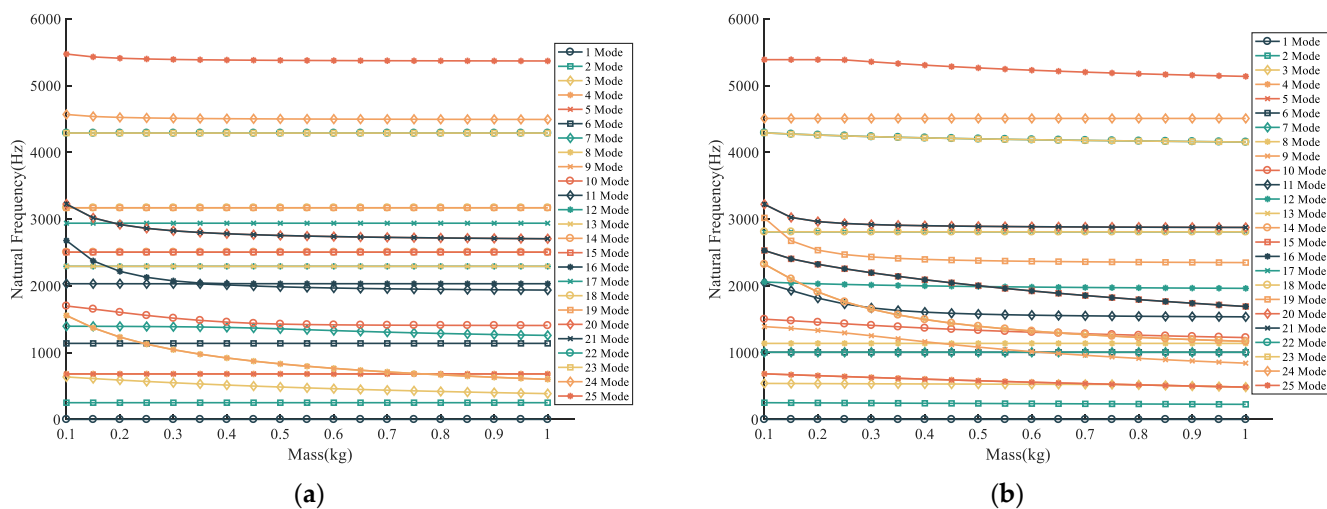


Figure 11. Sensitivity of the first 25 natural frequencies to the planet gear mass: (a) M_m ; (b) M_p .

Table 6. Vibration modes under variation in planet mass.

Mode	Fixed-Axis Train				Differential Train			
	$M_m = 0.1$ kg Nat. Freq. (Hz)	$M_m = 1$ kg Nat. Freq. (Hz)	Mod Type	Freq. Shift (%)	$M_p = 0.1$ kg Nat. Freq. (Hz)	$M_p = 1$ kg Nat. Freq. (Hz)	Mod Type	Freq. Shift (%)
1	0	0	couple	0	0	0	couple	0
2	249.96	249.96	couple	0	250.2	225.68	couple	9.8
3	635.37	385.58	couple	39.31	538.98	483.77	couple	10.24
4	680.52	680.52	differential train	0	682.74	483.77	differential train	29.14
5	680.52	680.52	differential train	0	682.74	483.77	differential train	29.14
6	1138.42	1138.42	planet carrier	0	1005.47	1005.47	fixed-axis train	0
7	1395.16	1257.79	couple	9.85	1005.47	1005.47	fixed-axis train	0
8	1556.41	599.63	fixed-axis train	61.47	1138.42	1138.42	planet carrier	0
9	1556.41	599.63	fixed-axis train	61.47	1389.59	842.26	couple	39.39
10	1698.55	1406.46	couple	17.2	1500.94	1225.51	couple	18.35
11	2031.74	1936.78	couple	4.67	2047.01	1536.29	couple	24.95
12	2292.34	2292.34	differential train	0	2058.29	1962.92	couple	4.63
13	2292.34	2292.34	differential train	0	2324.64	1168.2	differential train	49.75
14	2504.67	2504.67	differential train	0	2324.64	1168.2	differential train	49.75
15	2504.67	2504.67	differential train	0	2529.83	1691.2	differential train	33.15
16	2678.12	2031.99	couple	24.13	2529.83	1691.2	differential train	33.15
17	2938.39	2938.39	couple	0	2809.75	2809.75	fixed-axis train	0
18	3169.47	3169.47	differential train	0	2809.75	2809.75	fixed-axis train	0
19	3169.47	3169.47	differential train	0	3017.75	2348.77	couple	22.17
20	3224.87	2705.55	fixed-axis train	16.1	3221.6	2875.26	differential train	10.75
21	3224.87	2705.55	fixed-axis train	16.1	3221.6	2875.26	differential train	10.75
22	4288.77	4288.77	differential train	0	4291.78	4154.75	differential train	3.19
23	4288.77	4288.77	differential train	0	4291.78	4154.75	differential train	3.19
24	4567.2	4492.48	couple	1.64	4507.93	4507.88	couple	0
25	5472.18	5368.31	couple	1.9	5388.33	5137.52	couple	4.65

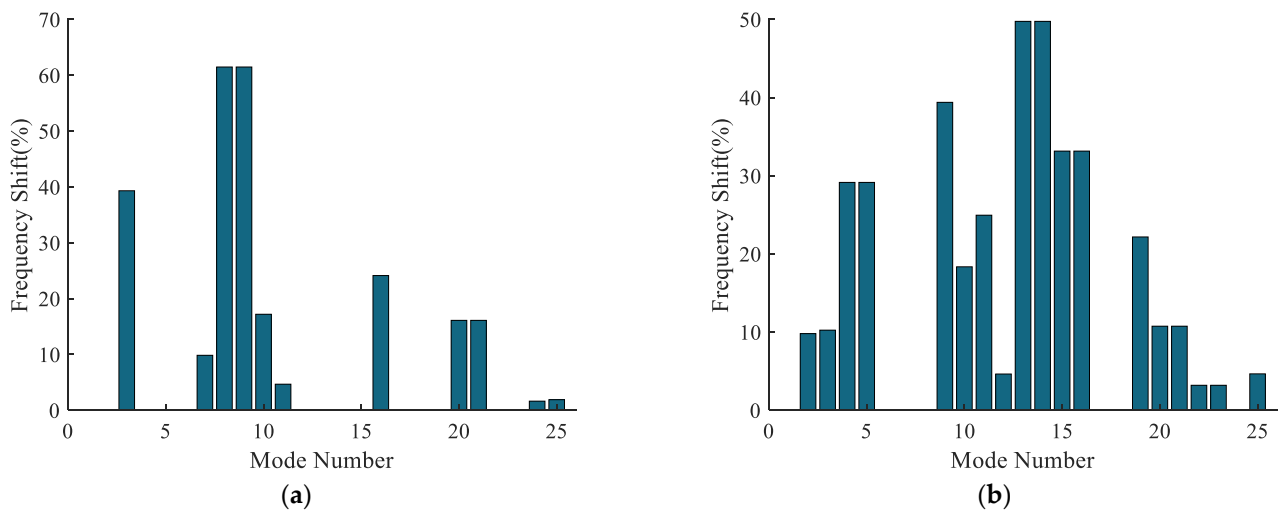


Figure 12. Frequency shifts for planet mass of 0.1 kg and 1 kg: (a) M_m ; (b) M_p .

From Table 6 and Figures 11 and 12, it can be seen that the effects of the planet mass on the natural frequencies are also very large, and the maximum value of the frequency shift reaches 61.47%. When M_m changes, the vibration modes corresponding to the changed natural frequencies are the fixed-axis train vibration mode and the coupled vibration mode; when M_p changes, the vibration modes corresponding to the changed natural frequencies are the differential train vibration mode and the coupled vibration mode. This also verifies the sensitivity of natural frequencies to the planet gear mass, as mentioned above. Similarly, the peak frequency shift generated by M_m is larger than that of M_p , but its influence affects fewer orders than M_p .

The mode transition phenomenon can be observed in Figure 11, and the mode transition in Figure 11a is verified by comparing the mode transition criterion in Table 4. There is no case1 in Figure 11a; frequencies (12, 13) are a double root, belonging to the differential train vibration mode, which are straight lines, verifying case2; frequencies (7, 10) are two single roots, belonging to the coupled vibration mode, and the transitions occur at 0.5 kg, verifying case3; frequencies (8, 9) are a double root, belonging to the fixed-axis train vibration mode, and frequency (6) is a single root, belonging to the coupled vibration mode, and intersections occur at 0.15 kg, verifying case4; frequency (16) is a single root, belonging to the coupled vibration mode, and it intersects with frequencies (12, 13) between 0.15 and 0.2 kg, which belong to the of the differential train vibration mode, verifying case5; frequencies (4, 5) are a double root, belonging to the differential train vibration mode, and intersect with frequencies (8, 9) between 0.75 and 0.8 kg, which belong to the fixed-axis train vibration mode, verifying case6. The mode transitions and intersections occurring at other positions in Figure 11a also conform to the mode transition criterion in Table 4, and similarly, the mode transitions and intersections in Figure 11b can be verified to conform to the mode transition criterion in Table 4, which is not repeated here.

4.4. Planet Rotational Inertia

Setting J_m from 10^{-4} kg·m² to 10^{-3} kg·m² and J_p from 10^{-5} kg·m² to 10^{-4} kg·m², the frequency shifts of the first 25 modes were calculated, as shown in Table 7. The sensitivity of the first 25 natural frequencies to the planet rotational inertia is shown in Figure 13, and the frequency shifts for extreme values of the rotational inertia are shown in Figure 14.

Table 7. Vibration modes under variation in planet rotational inertia.

Mode	Fixed-Axis Train				Differential Train			
	$J_m = 0.1$ kg Nat. Freq. (Hz)	$J_m = 1$ kg Nat. Freq. (Hz)	Mod Type	Freq. Shift (%)	$J_p = 0.1$ kg Nat. Freq. (Hz)	$J_p = 1$ kg Nat. Freq. (Hz)	Mod Type	Freq. Shift (%)
1	0	0	couple	0	0	0	couple	0
2	249.97	249.94	couple	0.01	250.18	249.59	couple	0.24
3	538.76	538.73	couple	0.01	539.47	537.49	couple	0.37
4	680.52	680.52	differential train	0	682.46	675.56	differential train	1.01
5	680.52	680.52	differential train	0	682.46	675.56	differential train	1.01
6	1014.34	959.12	fixed-axis train	5.44	1005.47	1005.47	fixed-axis train	0
7	1014.34	959.12	fixed-axis train	5.44	1005.47	1005.47	fixed-axis train	0
8	1138.42	1138.42	planet carrier	0	1138.42	1138.42	couple	0
9	1389.05	1358.09	couple	2.23	1388.53	1380.97	couple	0.54
10	1516.17	1438.54	couple	5.12	1499.92	1493.13	couple	0.45
11	2031.35	1872.99	couple	7.8	2030.7	2030.61	couple	0
12	2135.99	2031.66	couple	4.88	2054.82	2054.66	couple	0.01
13	2292.34	2292.34	differential train	0	2295.32	2276.9	differential train	0.8
14	2292.34	2292.34	differential train	0	2295.32	2276.9	differential train	0.8
15	2504.67	2504.67	differential train	0	2534.01	2424.1	differential train	4.34
16	2504.67	2504.67	differential train	0	2534.01	2424.1	differential train	4.34
17	2938.39	2938.39	couple	0	2809.75	2809.75	fixed-axis train	0
18	3169.47	3169.47	differential train	0	2809.75	2809.75	fixed-axis train	0
19	3169.47	3169.47	differential train	0	2938.39	2938.39	couple	0
20	3227.44	1868.08	fixed-axis train	42.12	3176.61	3148.44	differential train	0.89
21	3227.44	1868.08	fixed-axis train	42.12	3176.61	3148.44	differential train	0.89
22	4288.77	4288.77	differential train	0	4334.67	4111.9	differential train	5.14
23	4288.77	4288.77	differential train	0	4334.67	4111.9	differential train	5.14
24	4630.25	3855.18	couple	16.74	4520.8	4459.12	couple	1.36
25	5388.48	4613.61	couple	14.38	5388.38	5246.58	couple	2.63

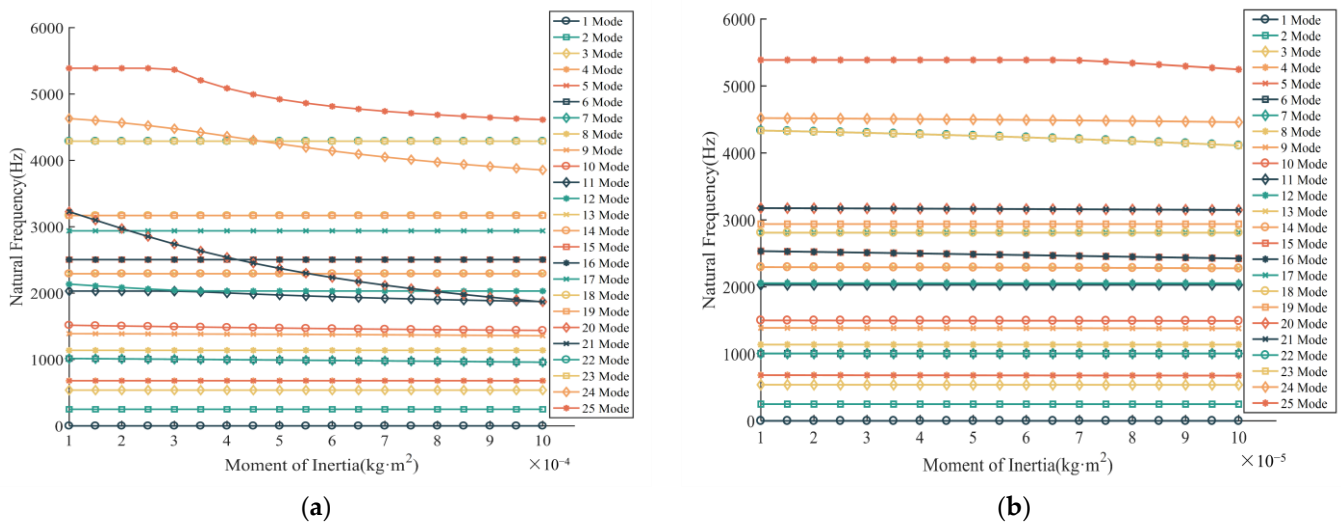


Figure 13. Sensitivity of the first 25 natural frequencies to the planet gear rotational inertia: (a) J_m ; (b) J_p .

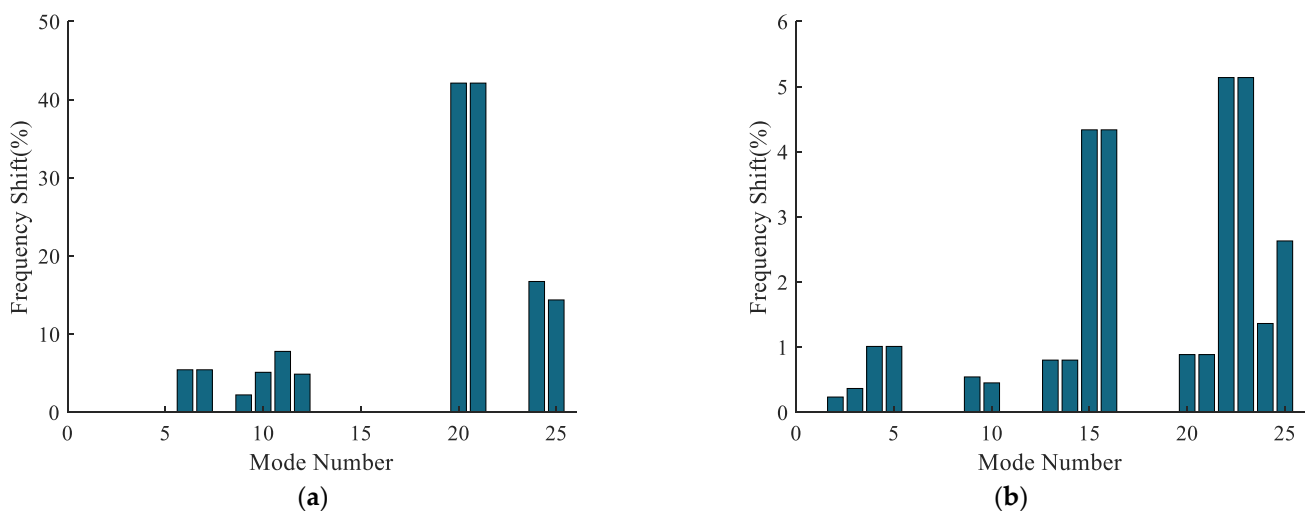


Figure 14. Frequency shifts for planet gear rotational inertia of extreme value. (a) J_m ; (b) J_p .

From Table 7 and Figures 12 and 13, it can be observed that due to J_m being an order of magnitude larger than J_p , the selected range for J_m also varies significantly. Within the chosen range of rotational inertia, the maximum frequency shift caused by J_m reaches 42.12%, while the maximum frequency shift caused by J_p is only 5.14%. As the rotational inertia changes, the sensitivity of the natural frequencies to the planet rotational inertia follows the expected rules as discussed earlier. Similarly, the order of occurrence frequency shift affected by J_m is less than that of J_p .

The mode transition phenomenon can be observed in Figure 13, and the mode transition in Figure 13a is verified by comparing the mode transition criterion in Table 4. There is no case1 in Figure 13a; frequencies (4, 5) are a double root, belonging to the differential train vibration mode, which are straight lines, verifying case2; frequencies (11, 12) are two single roots, belonging to the coupled vibration mode, and the transition occurs at $3.5 \times 10^{-4} \text{ kg}\cdot\text{m}^2$, verifying case3; frequencies (20, 21) are a double root, belonging to the fixed-axis train vibration mode, frequency (12) is a single root, belonging to the coupled vibration mode, and intersections occur between 7.5×10^{-4} and $8 \times 10^{-4} \text{ kg}\cdot\text{m}^2$, verifying case4; frequency (24) is a single root, belonging to the coupled vibration mode, frequencies (22, 23) are a double root, belonging to the vibration mode of the differential train, and intersections occur between 4.5×10^{-4} and $5 \times 10^{-4} \text{ kg}\cdot\text{m}^2$, verifying case5; frequencies (13,

14) are a double root, belonging to the differential train vibration mode, and intersect with frequencies (20, 21) between 5.5×10^{-4} and 6×10^{-4} kg·m², which belonging to the fixed-axis train vibration mode, verifying case6. The mode transitions and intersections occurring at the other positions in Figure 13a also conform to the mode transition criterion in Table 4. Within the selected mass range, the range of natural frequency variations in Figure 13b is small and does not reach the point where mode transitions and intersections occur.

5. Conclusions

Based on the centralized parameter model of the two-stage tandem hybrid planetary system, the natural characteristics were analyzed; three typical vibration modes were summarized; and the sensitivity of natural frequencies to unequally spaced planet, mesh stiffness, planet mass and rotational inertia, as well as the mode transition and intersection phenomena of natural frequencies under the influence of different parameters, were investigated.

(1) The vibration modes of the two-stage tandem hybrid planetary system include fixed-axis train vibration mode, differential train vibration mode and coupled vibration mode.

(2) The sensitivity of the natural frequencies to the parameters was investigated. With the change in the parameters in the fixed-axis train, the natural frequencies of the fixed-axis train vibration mode and the coupled vibration mode change, while the natural frequencies of the differential train vibration mode remain unchanged. With the change in parameters in the differential train, the natural frequencies of the differential train vibration mode and coupled vibration mode change, while the natural frequencies of the fixed-axis train vibration mode remain unchanged. Combined with the numerical examples, the correctness of the parameter sensitivity was verified, and the frequency shifts under the influence of different parameters were calculated.

(3) The mode transition phenomenon was investigated, and the criterion for the occurrence of mode transition of the two-stage tandem hybrid planetary system was determined, and the accuracy of the proposed mode transition criterion was verified by calculations.

Through the model established in this study, natural characteristics of the marine two-stage tandem hybrid planetary system can be swiftly obtained, aiding design engineers in better comprehending the dynamic behavior of the gear system. This understanding facilitates design optimization to mitigate resonance and enhance system performance, reliability and longevity. Despite the close resemblance between the mathematical model presented in this paper and finite element results, disparities from reality persist. Therefore, future research endeavors could involve further refining the model, such as the coupling between the sun gear and the planet gears at their respective ends, which could be explored in detail, treating the entire assembly as flexible components, among other aspects. It is anticipated that such refinements will yield results closer to reality, representing our forthcoming focus and dedication.

Author Contributions: Conceptualization, X.Z. and Z.Y.; methodology, X.Z. and Z.Y.; software, J.Q.; validation, M.D. and Y.W.; formal analysis, Z.Y.; investigation, Z.Y.; resources, X.Z.; data curation, M.D.; writing—original draft preparation, Z.Y.; writing—review and editing, Z.Y.; visualization, Y.W.; supervision, Y.W.; project administration, Y.W.; funding acquisition, Y.W. All authors have read and agreed to the published version of the manuscript.

Funding: This research was funded by the Technological Achievements Transformation Project, grant number CG21B010, and the Heilongjiang Provincial Nature Foundation research team project, grant number TD2023E002.

Data Availability Statement: The data presented in this study are available upon request from the corresponding author. The data are not publicly available due to laboratory regulations.

Conflicts of Interest: The authors declare no conflict of interest.

References

1. Ambarisha, V.K.; Parker, R.G. Nonlinear dynamics of planetary gears using analytical and finite element models. *J. Sound Vib.* **2007**, *302*, 577–595. [[CrossRef](#)]
2. Kahraman, A.; Blankenship, G.W. Interactions between commensurate parametric and forcing excitations in a system with clearance. *J. Sound Vib.* **1996**, *194*, 317–336. [[CrossRef](#)]
3. Zhao, R.Z.; Liu, H.; Zheng, Y.Q. Parameter sensitivity for the torsional vibration of wind turbine drive train system. In Proceedings of the International Conference on Information Science and Intelligent Control, Shanghai, China, 24–25 April 2015; pp. 71–76.
4. Zhang, L.; Wang, Y.; Wu, K.; Sheng, R.; Huang, Q. Dynamic modeling and vibration characteristics of a two-stage closed-form planetary gear train. *Mech. Mach. Theory* **2016**, *97*, 12–28. [[CrossRef](#)]
5. Wu, X.; Parker, R.G. Mode characteristics of planetary gears with an elastic continuum ring gear. *J. Appl. Mech.* **2008**, *75*, 031014. [[CrossRef](#)]
6. Sondkar, P.; Kahraman, A. A dynamic model of a double-helical planetary gear set. *Mech. Mach. Theory* **2013**, *70*, 157–174. [[CrossRef](#)]
7. Hao, D.; Zhi, L.; Jian, Z. Inherent characteristic analysis of a dual power split gear train. *IOP Conf. Ser. Earth Environ. Sci.* **2019**, *233*, 032007. [[CrossRef](#)]
8. Cui, T.; Li, Y.; Zan, C.; Chen, Y. Dynamic modeling and analysis of nonlinear compound planetary system. *Machines* **2022**, *10*, 31. [[CrossRef](#)]
9. Shuai, M.; Ting, Z.; Guo-Guang, J.; Xiao-Lin, C.; Han-Jun, G. Analytical investigation on load sharing characteristics of heringbone planetary gear train with flexible support and floating sun gear. *Mech. Mach. Theory* **2020**, *144*, 103670. [[CrossRef](#)]
10. Mbarek, A.; Hammami, A.; Del Rincon, A.F.; Chaari, F.; Rueda, F.V.; Haddar, M. Effect of load and mesh stiffness variation on mode characteristics of planetary gear. *Appl. Acoust.* **2019**, *147*, 32–43. [[CrossRef](#)]
11. Cooley, C.G.; Parker, R.G. Vibration properties of high-speed planetary gears with gyroscopic effects. *J. Vib. Acoust.* **2012**, *134*, 061014. [[CrossRef](#)]
12. Qiu, W.; Yang, F.; Wang, D.; Jiang, X. Design and free vibration characteristics of linkage planetary gear trains. *J. Braz. Soc. Mech. Sci. Eng.* **2022**, *44*, 58. [[CrossRef](#)]
13. Liu, H.; Zhan, Z. Modal properties of a two-stage planetary gear system with a Timoshenko beam as the intermediate shaft model. *Proc. Inst. Mech. Eng. Part D J. Automob. Eng.* **2022**, *236*, 353–365. [[CrossRef](#)]
14. Hu, Z.; Tang, J.; Wang, Q.; Chen, S.; Qian, L. Investigation of nonlinear dynamics and load sharing characteristics of a two-path split torque transmission system. *Mech. Mach. Theory* **2020**, *152*, 103955. [[CrossRef](#)]
15. Huang, C.; Huang, B.; Zhang, Y.; Xiao, K. Modal analysis and experimental research on a planetary reducer with small tooth number difference. *Trans. Can. Soc. Mech. Eng.* **2019**, *44*, 202–212. [[CrossRef](#)]
16. Hu, C.; Geng, G.; Liu, X.; Yang, S.; Tang, X. Dynamic Characteristics of the Multistage Planetary Gear Transmission System Based on a Stochastic Load. *Int. J. Precis. Eng. Manuf.* **2023**, *24*, 657–669. [[CrossRef](#)]
17. Tatar, A.; Schwingshackl, C.W.; Friswell, M.I. Dynamic behaviour of three-dimensional planetary geared rotor systems. *Mech. Mach. Theory* **2019**, *134*, 39–56. [[CrossRef](#)]
18. Tatar, A.; Schwingshackl, C.W.; Friswell, M.I. Modal sensitivity of three-dimensional planetary geared rotor systems to planet gear parameters. *Appl. Math. Model.* **2023**, *113*, 309–332. [[CrossRef](#)]
19. Guo, Y.; Parker, R.G. Sensitivity of general compound planetary gear natural frequencies and vibration modes to model parameters. *J. Vib. Acoust.* **2010**, *132*, 11006. [[CrossRef](#)]
20. Parker, R.G.; Wu, X. Vibration modes of planetary gears with unequally spaced planets and an elastic ring gear. *J. Sound Vib.* **2010**, *329*, 2265–2275. [[CrossRef](#)]
21. Cooley, C.G.; Parker, R.G. Eigenvalue sensitivity and veering in gyroscopic systems with application to high-speed planetary gears. *Eur. J. Mech.-A/Solids* **2018**, *67*, 123–136. [[CrossRef](#)]
22. Qian, P.-Y.; Zhang, Y.-L.; Cheng, G.; Ge, S.-R.; Zhou, C.-F. Model analysis and verification of 2K-H planetary gear system. *J. Vib. Control* **2015**, *21*, 1946–1957. [[CrossRef](#)]

Disclaimer/Publisher’s Note: The statements, opinions and data contained in all publications are solely those of the individual author(s) and contributor(s) and not of MDPI and/or the editor(s). MDPI and/or the editor(s) disclaim responsibility for any injury to people or property resulting from any ideas, methods, instructions or products referred to in the content.